PCP4 regulates Purkinje cell excitability and cardiac rhythmicity

Eugene E. Kim, Akshay Shekhar, Jia Lu, Xianming Lin, Fang-Yu Liu, Jie Zhang, Mario Delmar, and Glenn I. Fishman

Leon H. Charney Division of Cardiology, New York University School of Medicine, New York, New York, USA.

Cardiac Purkinje cells are important triggers of ventricular arrhythmias associated with heritable and acquired syndromes; however, the mechanisms responsible for this proarrhythmic behavior are incompletely understood. Here, through transcriptional profiling of genetically labeled cardiomyocytes, we identified expression of Purkinje cell protein-4 (*Pcp4*), a putative regulator of calmodulin and Ca^{2+}/calmodulin-dependent kinase II (CaMKII) signaling, exclusively within the His-Purkinje network. Using *Pcp4*-null mice and acquired cardiomyopathy models, we determined that reduced expression of PCP4 is associated with CaMKII activation, abnormal electrophysiology, dysregulated intracellular calcium handling, and proarrhythmic behavior in isolated Purkinje cells. *Pcp4*-null mice also displayed profound autonomic dysregulation and arrhythmic behavior in vivo. Together, these results demonstrate that PCP4 regulates cardiac excitability through both Purkinje cell–autonomous and central mechanisms and identify this modulator of CaMKII signaling as a potential arrhythmia-susceptibility candidate.

Introduction

Cardiac Purkinje cells (PCs) have been implicated in the genesis of ventricular arrhythmias in a variety of inherited conditions, such as long QT syndrome (1) and catecholaminergic polymorphic ventricular tachycardia (2), as well as acquired conditions, such as post–myocardial infarction (3) and dilated cardiomyopathy (4–6). The mechanisms responsible for this proarrhythmic propensity are incompletely understood, but compared with working ventricular myocytes (VMs), differences in T-tubular density (7), relative abundance of L and T type calcium channels (8), presence of IP_3-sensitive Ca^{2+} channels (9), greater intracellular sodium load (10), and the differential density of various repolarizing currents (11), are all considered contributory factors underlying the unique action potential (AP) and calcium-handling characteristics of PCs (12, 13). Triggered mechanisms have been proposed to underlie PC-related ventricular arrhythmias, and PCs have been found to be more susceptible to both early afterdepolarizations (EADs) and delayed afterdepolarizations (DADs) compared with working VMs (5, 14). The increased susceptibility of PCs to EADs is thought to result from AP prolongation and reactivation of depolarizing ionic currents, while the increased susceptibility to DADs is attributed, in part, to dysregulation of calcium homeostasis (14). However, the molecular basis for altered Purkinje electrophysiology and calcium homeostasis that predisposes to triggered activity remains incompletely elucidated.

With the goal of identifying novel regulators of PC electrophysiology that might lead to new targets for antiarrhythmic therapy, we performed a differential transcriptional screen of highly enriched populations of cardiac PCs and working ventricular cardiomyocytes. We report the discovery of Purkinje cell protein-4 (PCP4), a small IQ motif–containing protein that regulates calmodulin-dependent signaling and arrhythmogenicity through a cell-autonomous mechanism within the Purkinje fiber network. In addition, we found that PCP4 regulates cardiac rhythmicity through modulation of autonomic tone. Thus, *Pcp4* influences cardiac rhythmicity through both PC autonomous and central mechanisms.

Results

Expression of Pcp4 in the cardiac conduction system. To identify transcripts preferentially expressed in the Purkinje fiber network, dissociated cardiomyocytes from the ventricles of adult compound transgenic mice expressing PC (*Cntn2-EGFP*) and cardiomyocyte-specific (α-*MHC–Cre/ floxed tdTomato*) reporter genes (Figure 1A) were subjected to FACS (Figure 1B). Highly enriched populations of PCs ($Tomato^+EGFP^+$) and VMs ($Tomato^+EGFP^-$) were isolated and transcriptional profiling performed. Gene ontology functional analysis and canonical pathway analysis revealed numerous differences between the 2 cell types (Supplemental Figure 1; supplemental material available online with this article; doi:10.1172/JCI77495DS1). We identified marked enrichment of *Pcp4* in the PC population (Figure 1C). PCP4, also known as PEP-19, is a small IQ motif–containing protein of the calpacitin family of proteins and a negative regulator of calmodulin and Ca^{2+}/calmodulin-dependent kinase II–dependent (CaMKII-dependent) signaling in neurons (15–17). Results were validated by reverse-transcription PCR (RT-PCR) (Figure 1D) and quantitative PCR (qPCR) (Figure 1E), which confirmed that *Pcp4* was markedly enriched in PCs compared with VMs. Immunofluorescent staining of adult *Cntn2-EGFP* hearts demonstrated complete colocalization of PCP4 and EGFP in cardiomyocytes of the Purkinje fiber network (Figure 2A). Triple staining of more proximal elements of the cardiac conduction system (CCS) for the pacemaker channel protein HCN4 dem-

Authorship note: Eugene E. Kim and Akshay Shekhar contributed equally to this work.
Conflict of interest: The authors have declared that no conflict of interest exists.
Submitted: June 10, 2014; **Accepted:** September 4, 2014.
Reference information: *J Clin Invest*. 2014;124(11):5027–5036. doi:10.1172/JCI77495.

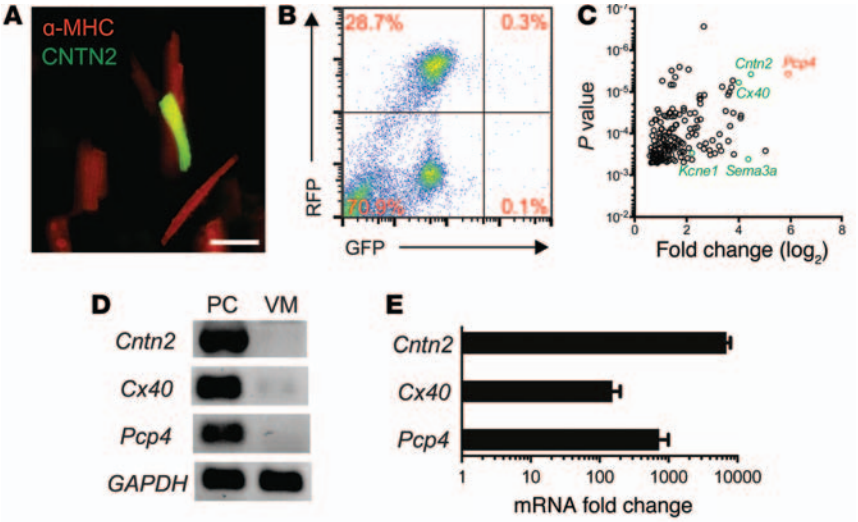

Figure 1. Identification of *Pcp4* gene expression within the Purkinje fiber network. (**A**) Fluorescence microscopy of isolated cells from *Cntn2-EGFP* / *α-MHC-Cre/floxed tdTomato* compound transgenic mouse identifies PCs expressing both cardiomyocyte (MHC) and PC (CNTN2) markers. Scale bar: 50 μm. (**B**) FACS dot plot reveals distinct PC (RFP^+GFP^+) and VM (RFP^+GFP^-) populations. Percentages of cells in each population are shown. (**C**) Gene-expression profiling of isolated PCs and VMs reveals *Pcp4* as one of the most highly enriched transcripts within the Purkinje fiber network ($n = 4$). (**D**) Semiquantitative and (**E**) quantitative RT-PCR analysis confirms marked enrichment of *Pcp4* along with other known markers of the ventricular conduction system (*Cx40*, *Cntn2*) in the PC fraction ($n = 3$). Data represent mean ± SEM.

onstrated abundant expression of PCP4 in the bundle of His, but virtually no expression in the atrioventricular node (AVN) (Figure 2B) or sinoatrial node (SAN) (Figure 2C). PCP4 also colocalized with CNTN2 in cardiac ganglia (Figure 2D). We also examined PCP4 expression in human ventricular myocardium, and as in the mouse heart, expression was restricted to the subendocardial Purkinje fiber network (Figure 2E).

PCP4 regulates CaMKII activity. The abundance of total CaMKII (tCaMKII) and its activity level as measured by threonine-287 phosphorylated CaMKII (pCaMKII) were assessed by quantitative immunofluorescence in *Pcp4*-null and control heart sections. In control hearts, the abundance of activated CaMKII was substantially increased in the Purkinje fiber network compared with immediately adjacent subendocardial working cardiomyocytes (Figure 3A). Additionally, a transmural gradient of activated CaMKII was observed within the working myocardium, with greater CaMKII activity in the midmyocardium compared with the subendocardial VMs (Figure 3, B and C). tCaMKII was also expressed in a gradient, with significantly less expression in the Purkinje fiber network compared with the working VMs of the midmyocardium (Figure 3, B and C). This pattern of expression of tCaMKII was unaltered in *Pcp4*-null hearts. However, in keeping with PCP4's putative negative regulatory role, expression of activated pCaMKII was markedly increased in the Purkinje fiber network of *Pcp4*-null mice compared with controls (Figure 3, B and C). As predicted, based on the lack of PCP4 expression in VMs, this effect was specific for PCs and there was no effect of loss of function of *Pcp4* on CaMKII activation in the working VM (Figure 3C). The CaMKII activation state was also assessed by evaluation of serine-2814 phosphorylation of the ryanodine receptor (RyR) (pSer2814-RyR), a CaMKII-dependent phosphorylation site. While no significant difference was seen in total RyR expression between PCs and VMs, greater abundance of pSer2814-RyR was observed in the Purkinje fiber network compared with working myocardium and in *Pcp4*-null PCs compared with WT PCs (Supplemental Figure 2). Again, no differences were seen between VMs of either genotype (Supplemental Figure 2). Taken together, these data indicate that constitutive activity of CaMKII is greater in PCs than in VMs and that loss of function of *Pcp4* relieves the inhibition of CaMKII activity exclusively within PCs.

PCP4 modulates PC electrophysiology. CaMKII regulates multiple ionic currents and the activities of numerous proteins responsible for intracellular calcium homeostasis, and therefore loss of function of *Pcp4* might be expected to modulate PC electrophysiology. To obtain an initial integrated measure of cardiac excitability, we used the whole-cell patch-clamp technique to record APs from adult WT and *Pcp4*-null PCs. Resting membrane potential and AP amplitude were no different between control and mutant PCs (Figure 4A). However, AP durations (APDs), determined at 50% (APD_{50}) and 90% (APD_{90}) repolarization, were both significantly prolonged in *Pcp4*-null PCs (Figure 4A). One of the principal targets of CaMKII implicated in APD prolongation is the pore-forming α subunit of the L-type Ca^{2+} channel. Indeed, we found a significant increase in I_{Ca} current density (Figure 4B) as well as a rightward shift in steady state inactivation (Figure 4C) in *Pcp4*-null PCs compared with WT controls. As predicted based upon the restricted pattern of PCP4 expression, no significant difference was seen in current density between mutant and control VMs (Supplemental Figure 3).

To determine whether the abnormalities in I_{Ca} in *Pcp4*-null PCs were mediated, either directly or indirectly, by dysregulated CaMKII activity, measurements of L-type Ca^{2+} currents were performed after treatment with autocamide-2–related inhibitory peptide (AIP), a specific inhibitor of CaMKII. Differences in I_{Ca} current density and steady state inactivation between mutant and WT PCs were abolished by AIP (Figure 4, B and C).

CaMKII also regulates intracellular Ca^{2+} cycling via phosphorylation of key proteins involved in the release and reuptake of Ca^{2+} from the sarcoplasmic reticulum. Accordingly, we measured Ca^{2+} transients in WT and *Pcp4*-null PCs and VMs by microfluorimetry. The exponential rate of decay of Ca^{2+} transients (τ) was significantly prolonged in mutant PCs compared with WT PCs (Figure 5, A and B), especially at slow pacing trains, resulting in a marked exaggeration of the frequency-dependent acceleration of relaxation (FDAR) index ($\tau_{5Hz}/\tau_{0.5Hz}$) in *Pcp4*-null PCs compared with WT PCs (Figure 5C). Consistent with this defect in Ca^{2+} handling, we also observed a marked accumulation of intracellular Ca^{2+} with repetitive stimulation in mutant PCs, particularly at faster pacing trains (Figure 5D). Again, no significant differences were observed

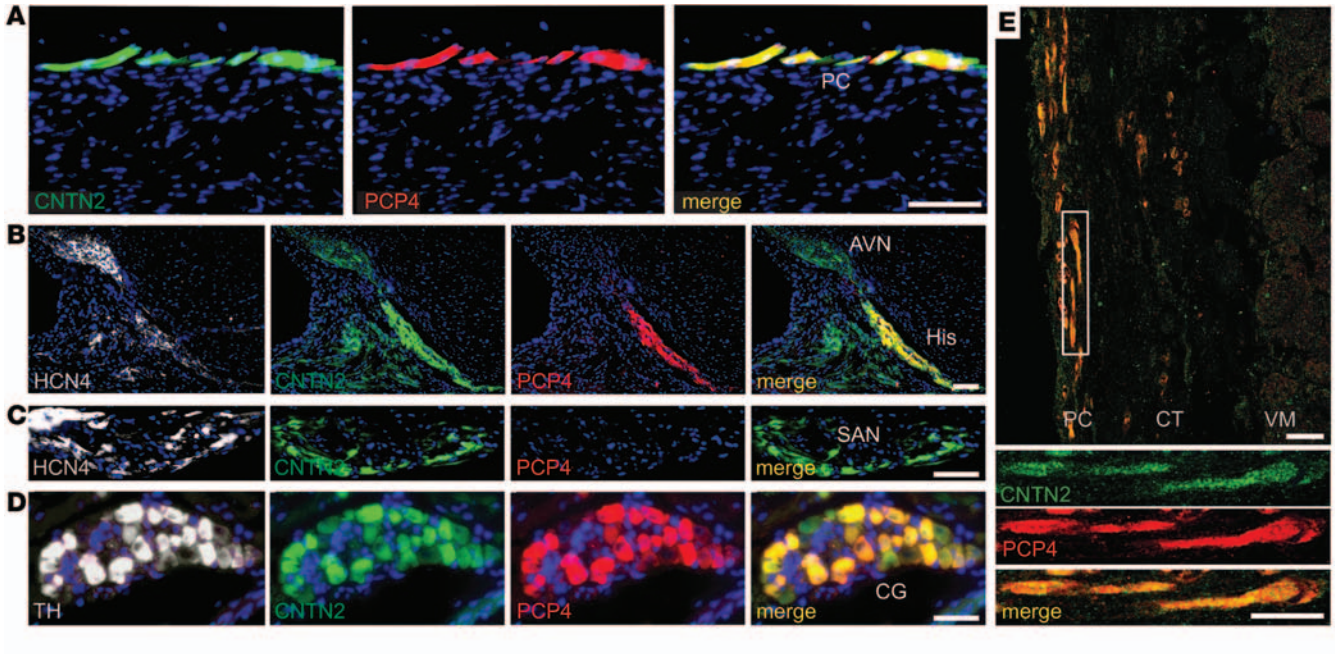

Figure 2. Immunolocalization of PCP4 within the ventricular conduction system and cardiac ganglia. (**A**–**D**) Immunofluorescence staining of PCP4 in *Cntn2-EGFP* heart sections. (**A**) PCP4 colocalizes with EGFP within subendocardial PCs. (**B**) HCN4 expression identifies the AVN and His bundle, which also express EGFP. In a serial section, PCP4 expression is seen only within the His bundle and excludes the AVN. (**C**) HCN4 expression identifies the SAN and colocalizes with EGFP. PCP4 expression is absent in a serial section of the SAN. (**D**) Tyrosine hydroxylase (TH) expression identifies cardiac ganglia (CG), in which robust PCP4 expression is detected. (**E**) CNTN2 and PCP4 colocalize to PCs in fetal human heart sections, which are separated from the working myocardium by a connective tissue sheath (CT). (18 weeks gestation). Scale bars: 50 μm.

between mutant and control VMs in Ca^{2+} transient characteristics (Supplemental Figure 4, A–C).

Pcp4-null PCs are highly arrhythmogenic. In agreement with our previous studies (2), PCs displayed significantly more spontaneous Ca^{2+} elevations (SCaEs) compared with VMs, including both early after-transients (EATs) (Figure 5E) and delayed after-transients (DATs) (Figure 5F). PCs from *Pcp4*-null mice demonstrated an even greater burden of SCaEs compared with WT controls. The difference in the frequency of EATs was most pronounced at slow pacing trains (Figure 5E), while the increased frequency of DATs was most pronounced at faster pacing trains (Figure 5F). Consistent with the absence of PCP4 expression outside of the His-Purkinje system, we observed no significant effect of genotype on SCaE frequency in VMs (Supplemental Figure 4D).

Exposure of PCs to AIP normalized the prolonged time constant of relaxation (Figure 5B) as well as the FDAR index (Figure 5C). CaMKII inhibition also blunted the accumulation of intracellular Ca^{2+} in both WT and mutant PCs, with no significant difference in diastolic-free Ca^{2+} after repetitive stimulation in either cell type (Figure 5D). Finally, in the presence of AIP, no EATs were observed in either WT or *Pcp4*-null PCs (Figure 5E) and the burden of DATs was dramatically reduced, such that there was no significant difference in frequency between WT and mutant PCs (Figure 5F).

PCP4 is downregulated in acquired disease models. To determine whether altered expression of PCP4 may play a mechanistic role in PC-dependent arrhythmic activity in acquired forms of heart disease, we employed 2 well-established disease models, i.e., phenylephrine (PE) infusion via osmotic mini-pump and transverse aortic constriction. Both stressors resulted in echocardiographic evidence of structural remodeling and contractile deficits (Supplemental Table 1). Quantitative immunofluorescent staining of ventricular myocardium demonstrated substantial downregulation of PCP4 in the PCs of both disease models (Figure 6, A and C). Furthermore, consistent with the finding in *Pcp4*-null mice, downregulation of PCP4 was associated with significantly increased pCaMKII expression, both in PCs and the working myocardium (Figure 6, B and C). PCs isolated from diseased hearts developed many of the same functional abnormalities as those observed in *Pcp4*-null PCs, including prolongation of τ (Figure 7A) and exaggerated FDAR (Figure 7B), increased intracellular Ca^{2+} accumulation (Figure 7C), and increased frequency of both EATs (Figure 7D) and DATs (Figure 7E). Taken together, these data support the hypothesis that PCP4 physiologically inhibits CaMKII activity in PCs and genetic loss of function or acquired downregulation of PCP4 relieves this inhibition, resulting in dysregulated intracellular Ca^{2+} handling and proarrhythmic behavior.

Cardiac arrhythmias in Pcp4-null mice. In order to examine the effect of *Pcp4* deletion in vivo, ECGs and echocardiograms were performed on anesthetized *Pcp4*-null and WT mice, which revealed no significant differences in baseline electrocardiographic parameters, cardiac size, or contractility (Supplemental Tables 1 and 2). Given the aberrant intracellular Ca^{2+} handling observed in the *Pcp4*-null mice, we examined the effects of further provoking PC Ca^{2+} dynamics. Pharmacologic challenge of anesthetized WT mice with caffeine and epinephrine resulted in sinus tachycardia with rare premature ventricular complexes (PVCs) (Figure 8A). In contrast, mutant mice developed frequent PVCs (Figure 8, B, F, and G), monomorphic ventricular tachycardia (Figure 8, C and

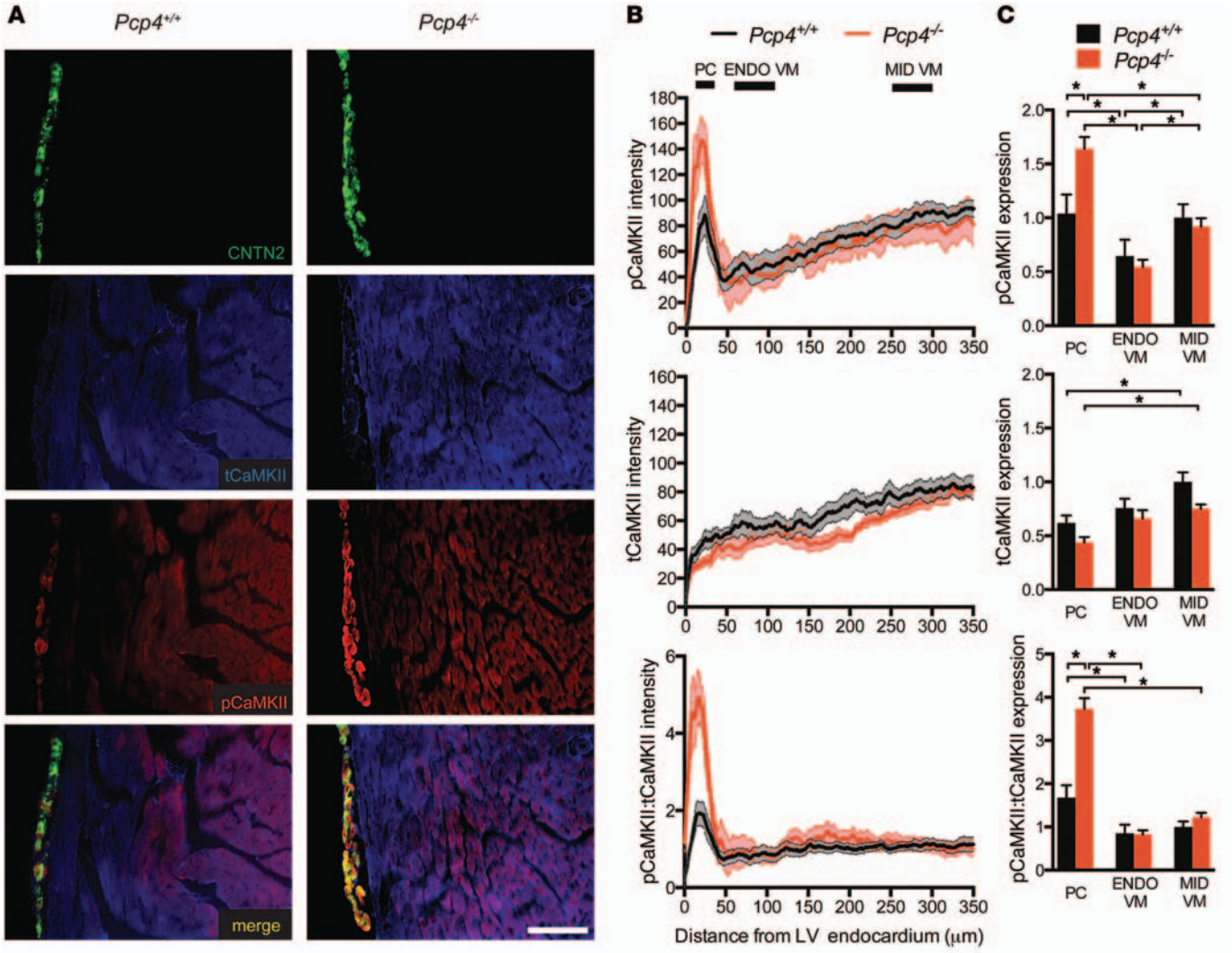

Figure 3. Transmural expression patterns of tCaMKII and pCaMKII in *Pcp4*-null and control hearts. (**A**) Representative immunofluorescence staining of tCaMKII and pCaMKII in *Pcp4*-null and control hearts. CNTN2 expression identifies PCs. (**B** and **C**) Quantitative assessment of the abundance of pCaMKII and tCaMKII and the ratio of pCaMKII/tCaMKII as assessed by pixel intensity. (**B**) Intensity measurements were plotted (in arbitrary units) as a function of distance from the endocardium in the left ventricular free-wall myocardium. (**C**) Comparison of intensity measurements (plotted in arbitrary units) within distinct compartments of *Pcp4*-null and control animals: Purkinje network (PC; 10–40 μm from endocardium), subendocardial VMs (ENDO VM; 75–125 μm from endocardium), and midmyocardial VMs (MID VM; 250–300 μm from endocardium). Scale bar: 100 μm. Data represent mean ± SEM. $^*P < 0.05$.

G), bidirectional ventricular tachycardia (Figure 8, D and G, and Supplemental Figure 5A), and aberrant ventricular conduction (Figure 8, E and G). Unexpectedly, in all mutant mice, this surge of ventricular ectopy was followed by marked sinus arrhythmia, frequent sinus pauses (Figure 9, A and B) and first-degree and second-degree Mobitz type 1 heart block (Supplemental Figure 5B). Moreover, while WT mice recovered uneventfully from anesthesia, all *Pcp4*-null mice died during withdrawal of anesthesia from sinus bradycardia that progressed to complete heart block and asystole (Figure 9C). Given the absence of detectable PCP4 in the SAN or AVN but its presence in cardiac autonomic ganglia, this response suggested that PCP4 might influence cardiac rhythmicity through modulation of autonomic tone. Indeed, administration of atropine with caffeine and epinephrine prevented periodic heart rate slowing and lethal bradycardic response in all mutant mice tested (Supplemental Figure 5C), implicating a vagal surge as the mechanism of death. To further investigate this potential autonomic dysregulation in *Pcp4* mutant mice, continuous ambulatory ECG recordings were performed. While there were no significant differences in average heart rate or diurnal heart rate patterns (Figure 9, D and E), there was a marked increase in heart rate variability (HRV) in the mutant mice (Figure 9, E and F). These findings were most evident at night, when mice were active. Treatment with atropine resulted in complete normalization of HRV in *Pcp4*-null mice (Figure 9, G and H).

Discussion

The mechanisms responsible for the increased arrhythmogenic behavior of cardiac PCs are incompletely understood. In the present study, we report that PCP4, a small IQ motif–containing protein of the calpacitin family of proteins originally identified in cerebellar PCs, is preferentially expressed within the ventricular

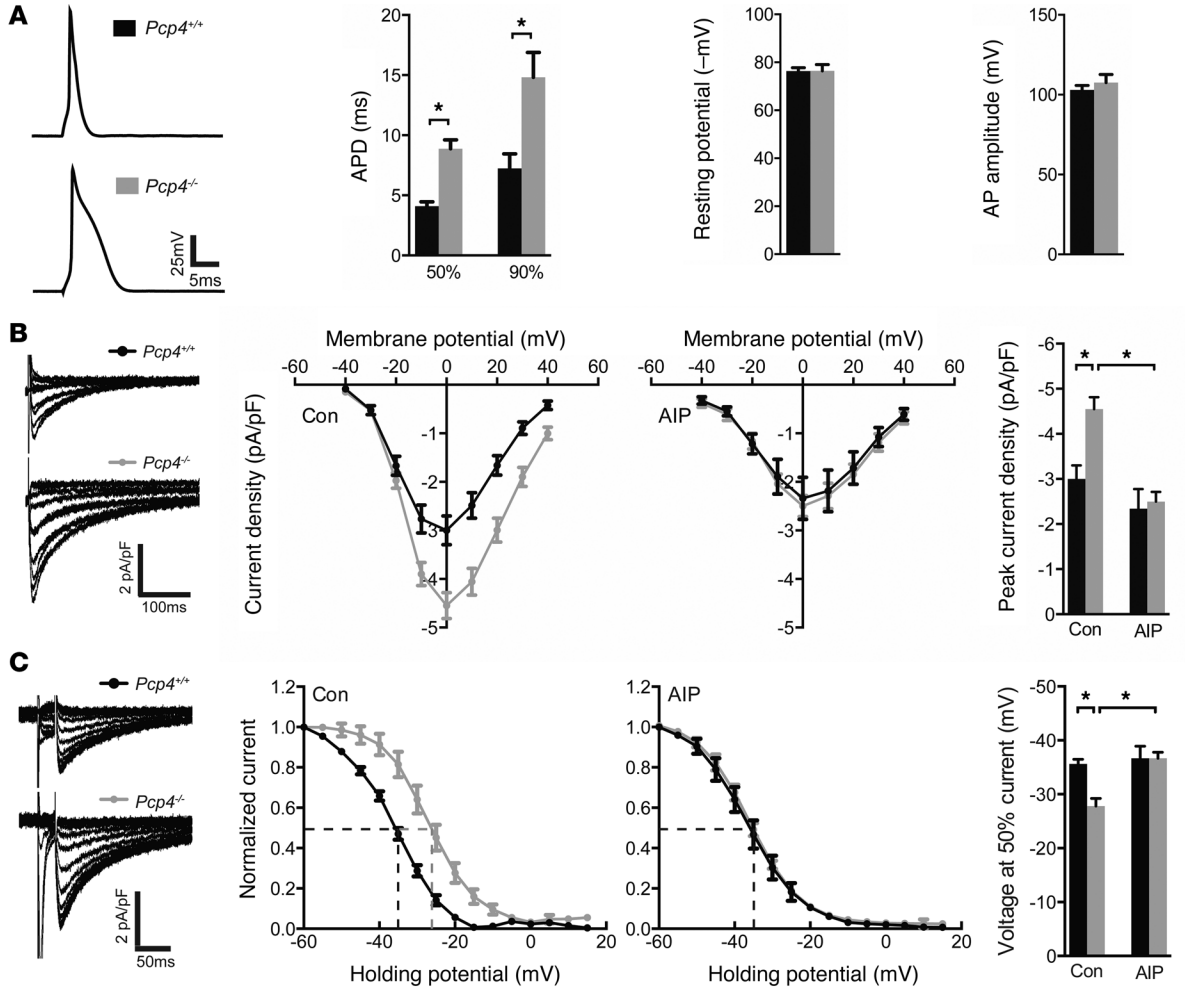

Figure 4. Effect of *Pcp4*-null mutation on PC AP characteristics and calcium currents. (**A**) Representative AP tracings from control and *Pcp4*-null PCs. Comparison of APD_{50} and APD_{90} of repolarization, resting membrane potential and AP amplitude between *Pcp4*-null and control PCs. (**B**) Comparison of current-voltage (I-V) relationship of I_{Ca} in *Pcp4*-null and control PCs in the presence or absence of AIP. Peak current density was plotted and used to assess significant differences among experimental groups. Representative whole-cell recordings of I_{Ca} evoked by voltage steps from –40 to +40 mV in 10-mV increments from a holding potential of –50 mV with a 30-ms prepulse to –30 mV. (**C**) Comparison of steady state inactivation curve of I_{Ca} in *Pcp4*-null and control PCs in the presence or absence of AIP. The voltage at half-inactivation ($V_{1/2}$) was plotted and used to assess significant differences among experimental groups. Representative whole-cell recordings of I_{Ca} evoked by voltage clamp at 0 mV after a 30-ms prepulse to –30 mV from holding potentials stepped from –60 to +15 mV for 1 second in 5-mV increments. For **A**–**C**, n = 10–15 cells per group. Data represent mean ± SEM. *$P < 0.05$.

CCS, where it regulates cardiac PC electrophysiology and intracellular calcium handling in a CaMKII-dependent manner. Moreover, using genetic and acquired models of heart disease, we show that downregulation of PCP4 is associated with enhanced CaMKII activity in PCs, resulting in proarrhythmic behavior. Finally, we demonstrate that PCP4 regulates cardiac rhythmicity through modulation of autonomic tone.

We identified *Pcp4* through comparative transcriptional profiling of ventricular cardiomyocytes using *Cntn2-EGFP* reporter mice. Among the conduction system markers we and others have previously described, including *CCS-lacZ*, *Cx40*, *HCN4*, *minK*, and *Cntn2-EGFP*, *Pcp4* is unique to date in that expression within the cardiomyocyte lineage appears restricted to the ventricular conduction system, i.e., the His-Purkinje network, with no detectable expression more proximally in the SA or AV nodes. The mechanisms that facilitate this highly circumscribed expression pattern are unknown; however, a combination of in silico and direct experimental strategies should begin to unravel the relevant transcriptional circuitry. Regardless of underlying mechanisms, genetically engineered models utilizing *Pcp4* regulatory elements should be useful in examining ventricular conduction system development and function in health and disease.

PCP4 binds calmodulin, increasing the Ca^{2+}-binding rate constants of this calcium sensor by 50-fold. Calmodulin has been described as an ion channel subunit due to its ability to interact with and regulate the function of a number of important ion channels, including the LTCC, RyR, IP_3-sensitive channels, and calcium-activated potassium channels (18). By influencing the kinetics of calmodulin-Ca^{2+} binding, PCP4 has the potential to affect cellular electrophysiology via modulation of calmodulin-mediated channel gating. In neurons, where PCP4 is best characterized, it also is thought to regulate cellular physiology through modulation of the Ca^{2+}/calmodulin-dependent enzyme CaMKII (15–17). Given the accumulating evidence implicating dysregulated

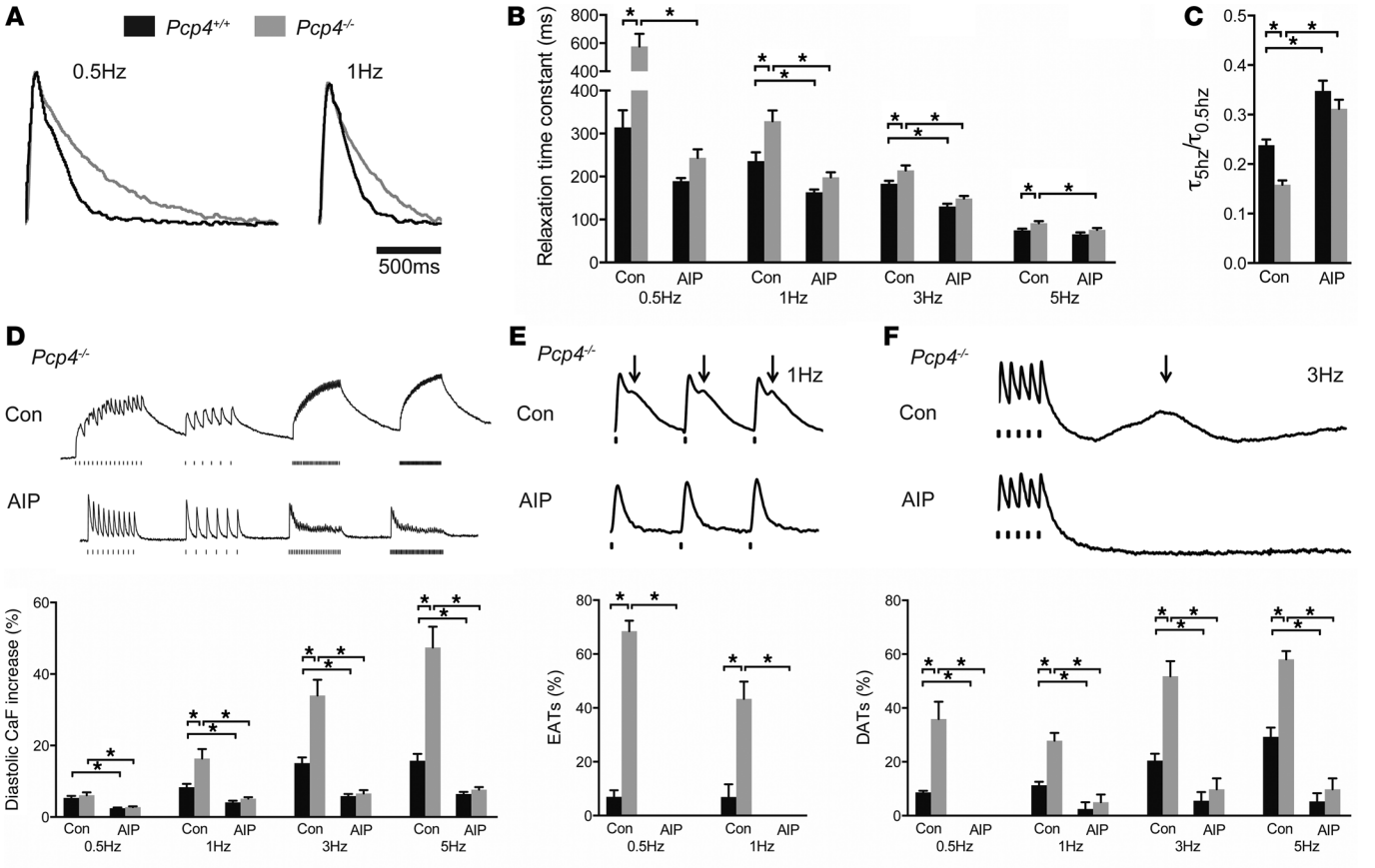

Figure 5. Effect of *Pcp4*-null mutation on PC calcium cycling. (**A**) Averaged calcium transients of *Pcp4*-null and control PCs. (**B** and **C**) Kinetics of intracellular calcium decay. (**B**) The relaxation time constant (τ) at various stimulation frequencies and (**C**) the FDAR index ($\tau_{5Hz}/\tau_{0.5Hz}$) between *Pcp4*-null PCs and control PCs in the presence or absence of AIP. (**D**–**F**) Representative calcium transient recordings and comparison of (**D**) the intracellular calcium concentration with repetitive stimulation, (**E**) the frequency of EATs, and (**F**) the frequency of delayed DATs between PCs of *Pcp4*-null and control mice at various stimulation frequencies in the presence or absence of AIP. Con, vehicle. For **A**–**D**, *n* = 30–45 cells per group. For **E** and **F**, *n* = 4–6 hearts per group. 8–12 cells were recorded from each heart. Data represent mean ± SEM. $^*P < 0.05$.

CaMKII activity in inherited and acquired forms of arrhythmogenic heart disease (19) as well as the recent identification of a number of calmodulin mutations associated with long QT syndromes, CPVT, and sudden death (20, 21), PCP4 represented an especially attractive candidate as an important modulator of cardiac PC electrophysiology.

CaMKII has profound effects on membrane excitability via regulation of many voltage-gated ion channels, resulting in prolongation of the AP and enhanced susceptibility to EADs (19, 22, 23). Additionally, Ca^{2+}-cycling proteins critical for the normal release and reuptake of Ca^{2+} from the sarcoplasmic reticulum are targets of CaMKII. Pathological phosphorylation of these proteins by CaMKII favors cytosolic Ca^{2+} excess, activation of the electrogenic Na^{+}-Ca^{2+} exchanger (NCX), and DAD formation (19, 24). Indeed, we observed many of these cellular abnormalities in *Pcp4*-null PCs, and their amelioration by AIP implies a mechanistic role for CaMKII in the disease phenotype.

Surprisingly, the effect of PCP4 on cardiac rhythmicity appears quite complex and mediated by PC-autonomous as well as autonomically mediated effects. While *Pcp4*-null mice showed a greater burden of ventricular arrhythmias and aberrant ventricular conduction consistent with the proarrhythmic cellular remodeling seen in isolated cells, our telemetric recordings also suggested that PCP4 influences cardiac rhythmicity through a non–cell autonomous mechanism involving modulation of autonomic tone. Indeed, the most dramatic abnormality we observed was the lethal bradycardia seen during withdrawal of anesthesia after adrenergic challenge. Since no PCP4 expression was detected in the SA or AV node, this finding is not directly attributable to a cardiomyocyte-autonomous effect of PCP4, but instead, likely reflects loss of PCP4 in the autonomic nervous system. Consistent with this hypothesis, we detected robust expression of PCP4 in cardiac ganglia and a complete abrogation of lethality with vagal antagonism. Interestingly, CaMKII-dependent signaling has been implicated in synaptic plasticity in autonomic ganglia and the regulation of autonomic tone (25). Lineage-restricted gene targeting will be required to formally distinguish PC-autonomous from autonomically mediated effects of PCP4 on cardiac rhythmicity.

Interestingly, PCP4 is reportedly downregulated in selected brain regions in a number of neurologic syndromes, including Parkinson disease (26), Huntington disease (27), and chronic alcoholism (28). Moreover, a genetic mouse model of Huntington disease phenocopies the autonomic dysregulation seen in the *Pcp4*-null

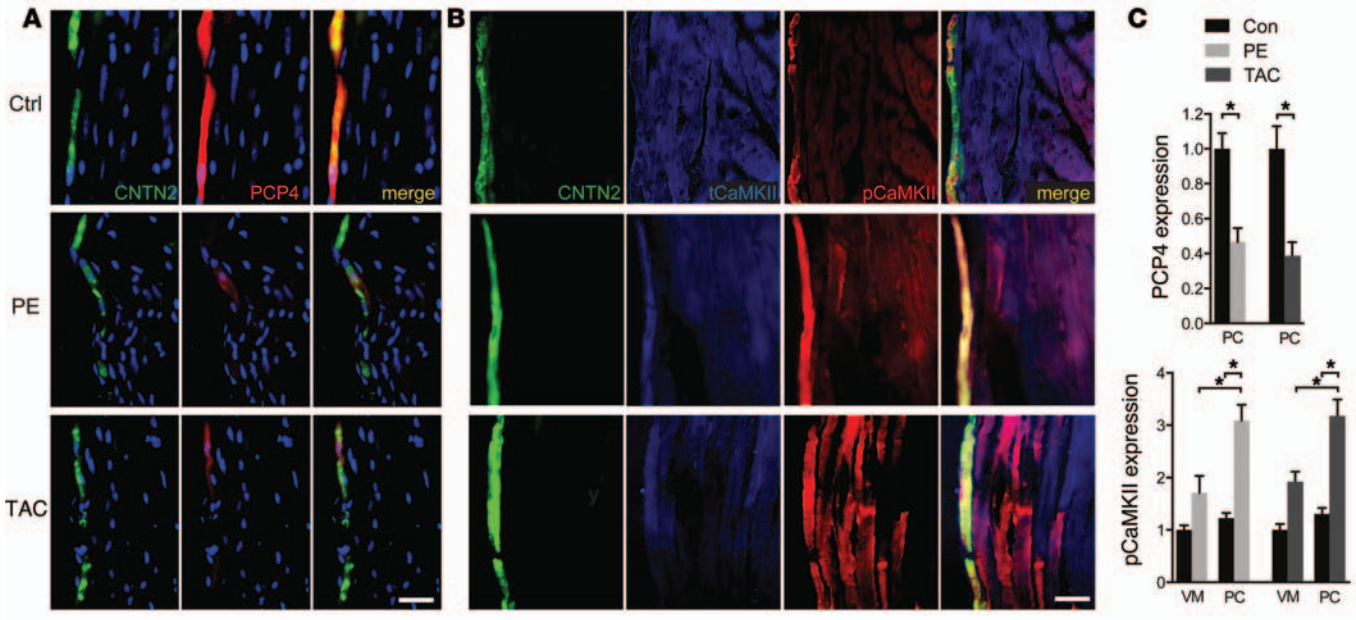

Figure 6. Altered expression of PCP4 and pCaMKII in cardiac disease models. (**A** and **B**) Representative immunofluorescence staining for (**A**) PCP4 and (**B**) tCaMKII and pCaMKII in heart sections from control animals and animals treated with PE via osmotic minipump for 1 week (PE) or transverse aortic constriction for 6 weeks (TAC). CNTN2 expression identifies PCs. (**C**) Comparison of quantitative immunofluorescence intensity for PCP4 within PCs and pCaMKII within VMs and PCs from control, PE, or TAC animals. Scale bars: 50 μm. Data represent mean ± SEM. *$P < 0.05$.

animals (29). It is tantalizing to speculate that PCP4 downregulation may play a mechanistic role in the autonomic dysregulation observed in selected neurologic syndromes.

In summary, we have identified PCP4 as a protein expressed in the Purkinje fiber network that regulates cellular electrophysiology and calcium homeostasis through inhibition of CaMKII activity. Downregulation of *Pcp4* expression in disease states relieves this inhibition and promotes triggered activity and arrhythmic behavior. PCP4 is also found in cardiac ganglia, where it potently influences cardiac rhythmicity through modulation of autonomic tone. Thus, *Pcp4* may represent a new arrhythmia-susceptibility gene, and preservation of PCP4 activity in disease states may diminish both Purkinje-triggered and vagally-mediated arrhythmic behavior.

Methods

Mutant mice. *Cntn2-EGFP* BAC transgenic (2), α-MHC-Cre (30), floxed tdTomato (31), and *Pcp4*-null (32) mutant mice (provided by James Morgan, St. Jude Children's Research Hospital, Memphis, Tennessee, USA) have all been previously described. *Cntn2-EGFP* mice were maintained in a CD1 genetic background. *Pcp4*-null mice were maintained in a C57BL/6-129S hybrid background. For functional studies of PCs, *Pcp4*-null mice were bred into the *Cntn2-EGFP* background. All functional studies were performed on male mice from

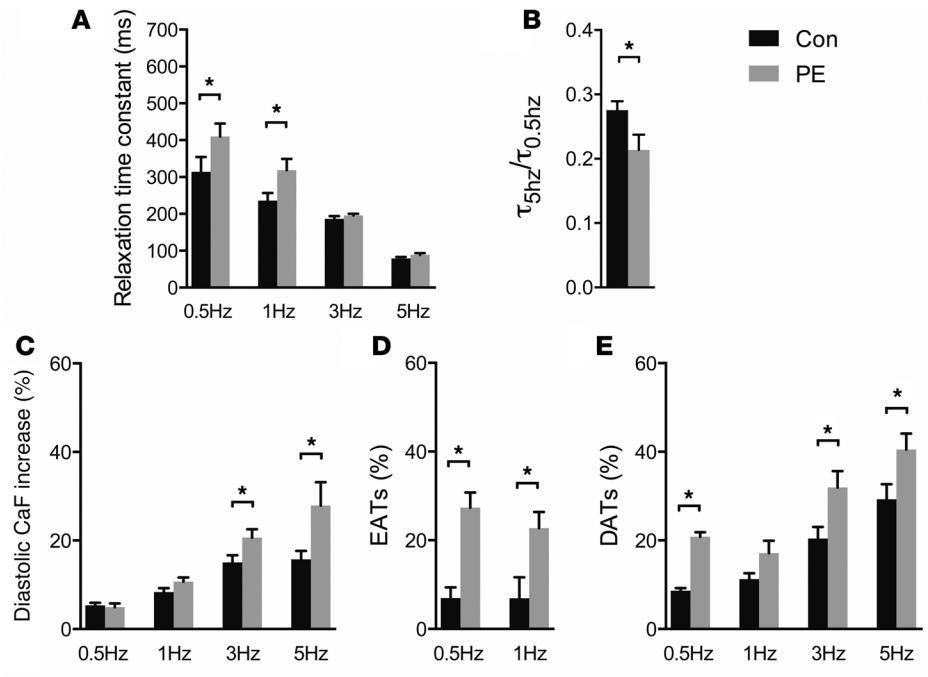

Figure 7. Abnormal PC calcium cycling in PE-induced cardiac hypertrophy. (**A**–**E**) Comparison of PC calcium-cycling dynamics in PE-treated versus control animals. (**A**) The relaxation time constant (τ) at various stimulation frequencies. (**B**) The FDAR index ($\tau_{5Hz}/\tau_{0.5Hz}$). (**C**) The intracellular calcium concentration with repetitive stimulation. (**D**) The frequency of EATs and (**E**) DATs. For **A**–**C**, n = 20–30 cells per group. For **D** and **E**, n = 3 hearts per group. 8–12 cells were recorded from each heart. Data represent mean ± SEM. *$P < 0.05$.

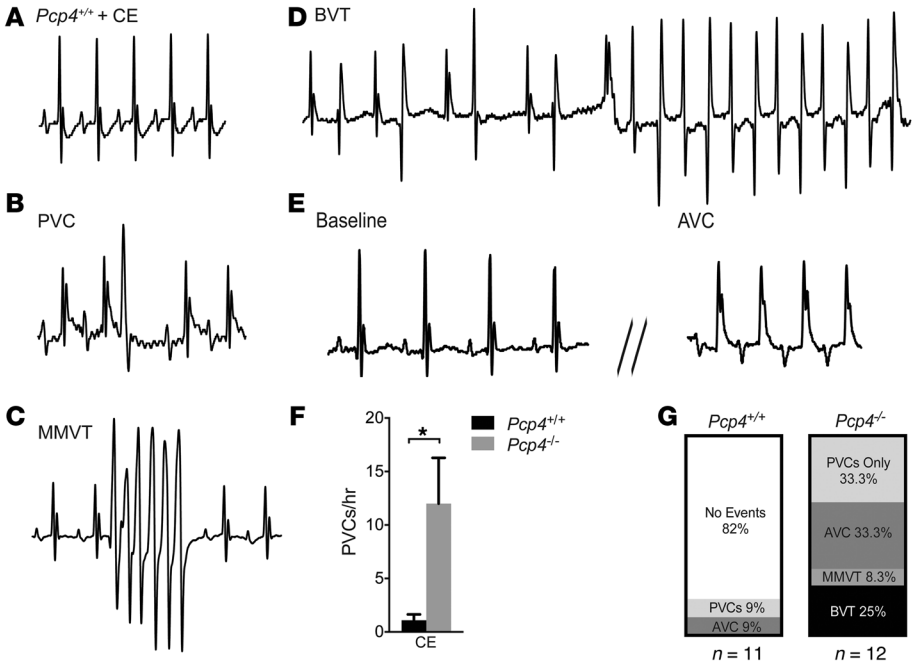

Figure 8. *Pcp4-null* mice are prone to ventricular arrhythmias and aberrant ventricular conduction. (**A**–**E**) Representative ECG tracings from anesthetized mice after administration of caffeine and epinephrine (CE). (**A**) *Pcp4*$^{+/+}$ control mouse ECG demonstrates sinus tachycardia without ventricular ectopy. (**B**–**E**) *Pcp4*$^{-/-}$ mutant mouse ECGs demonstrate (**B**) isolated PVC; (**C**) monomorphic ventricular tachycardia (MMVT); (**D**) bidirectional ventricular tachycardia (BVT); and (**E**) aberrant ventricular conduction (AVC). (**F**) Comparison of PVC frequency between *Pcp4*$^{+/+}$ and *Pcp4*$^{-/-}$ mice after caffeine and epinephrine. (**G**) Proportion of *Pcp4-null* mice that developed ventricular arrhythmias or AVC after caffeine and epinephrine ($n > 11$). Data represent mean ± SEM. $^*P < 0.05$.

F2–4 crosses between the 2 strains and used at 8 to 16 weeks of age. To minimize experimental variability, data from VMs and PCs from the same preparation were always collected on the same day.

Gene transcriptional profiling and RT-PCR. Cardiac cells were dissociated from adult hearts via Langendorff perfusion and enzymatic digestion as previously described (2) and sorted by FACS (Beckman Coulter MoFlo). RNA was isolated from sorted cell populations using the PicoPure RNA Isolation Kit (Arcturus). Isolated RNA was amplified using the Ovation Pico WTA System V2 (Nugen), and transcriptional profiling was performed using Mouse Genome 430 2.0 Array (Affymetrix). All original microarray data were deposited in the NCBI's Gene Expression Omnibus (GEO GSE60987). Data analysis was performed using robust multi-array average (RMA) followed by linear models for microarray data (LIMMA) to identify differentially expressed transcripts with a false discovery rate (FDR) of 0.05. PCR was performed on amplified cDNA using the Quantitect SYBR Green PCR Kit (QIAGEN).

Immunohistochemistry. Hearts were excised from animals anesthetized with ketamine (120 mg per kg body weight i.p.) and xylaxine (10 mg per kg body weight i.p.). Excised hearts were fixed overnight in 4% paraformaldehyde and cryosections prepared and stained as previously described (13). Immunostaining of cryosections from cadaveric fetal human tissues fixed in 10% neutral buffered formalin was performed. Primary antibodies were directed against PCP4 (1:500; provided by James Morgan), HCN4 (1:100, AB5808; Millipore), tyrosine hydroxylase (1:100, AB152; Millipore), contactin 2 (1:40, AF4439; R&D Systems), CaMKII (1:50, ab22609; Abcam;), pCaMKII (1:500, ab32678; Abcam), RyR2 (1:100, AB9080; Millipore), pSer2814-RyR2 (1:100, A010-31; Badrilla), and troponin T (1:100, MS-295; Thermo) and visualized by epifluorescence (Zeiss) or confocal (Leica) microscopy. Quantitation of immunofluorescence was performed using ImageJ (http://imagej.nih.gov/ij/). Multiple plot profiles of pixel intensity generated from transmural sections were averaged in order to quantify intensity as a function of distance from endocardium. Additionally, specific regions for PCs (10–40 μm from endocardium), subendocardial VMs (75–125 μm from endocardium), and midmyocardial ventricular myocytes (250–300 μm from endocardium) were defined, and after exclusion of intercellular spaces, average pixel intensity for each region was determined. Images were obtained from a minimum of 25 sections from at least 3 hearts from each genotype or treatment group.

Calcium imaging and voltage measurements. Adult myocytes were isolated using enzymatic digestion, and intracellular Ca^{2+} imaging was performed using X-Rhod 1 dye (2.5 μM) and a microfluorimetry system (IonOptix Corp.) as previously described (2). The SCaEs were defined as unstimulated increases in intracellular Ca^{2+}. Delayed aftertransients were quantified during the 10-second unpaced interval following the 10-second pacing train. For CaMKII inhibitor experiments, cell-permeable AIP (1 μmol/l; Calbiochem) was loaded into cells for a minimum of 1 hour prior to functional experiments. Adult ventricular cardiomyocyte APs were obtained with whole-cell current clamp mode. The recording pipette solution contained the following: 135 mM KCl, 1 mM $MgCl_2$, 10 mM EGTA, 10 mM HEPES, and 5 mM glucose, pH 7.2, with KOH. The bath solution contained the following: 136 mM NaCl, 4 mM KCl, 1 mM $CaCl_2$, 2 mM $MgCl_2$, 10 mM HEPES, and 10 mM glucose, pH 7.4, with NaOH. A brief current pulse (up to 3 ms duration) at approximately twice the voltage threshold for excitation was used to evoke APs at a cycle length of 1 s (1 Hz). APD_{50} and APD_{90} repolarization were measured using Clampfit version 10.0. For calcium current experiments, the recording pipette solution contained the following: 120 mM CsCl, 20 mM TEACl, 1 mM $MgCl_2$, 10 mM EGTA, 10 mM HEPES, 5 mM Mg-ATP, 0.2 mM Na_2-GTP (pH adjusted to 7.2 with CsOH). The bath solution contained the following: 137.7 mM NaCl, 5.4 mM CsCl, 1 mM $CaCl_2$, 1 mM $MgCl_2$, 10 mM glucose, 10 mM HEPES, and 2 mM4-aminopyridine (pH adjusted to 7.4 with NaOH). The resistances of the electrodes were maintained between 2 and 4 mega-ohms. The following pulse protocols were used to generate current-voltage relationship and steady state inactivation curves.

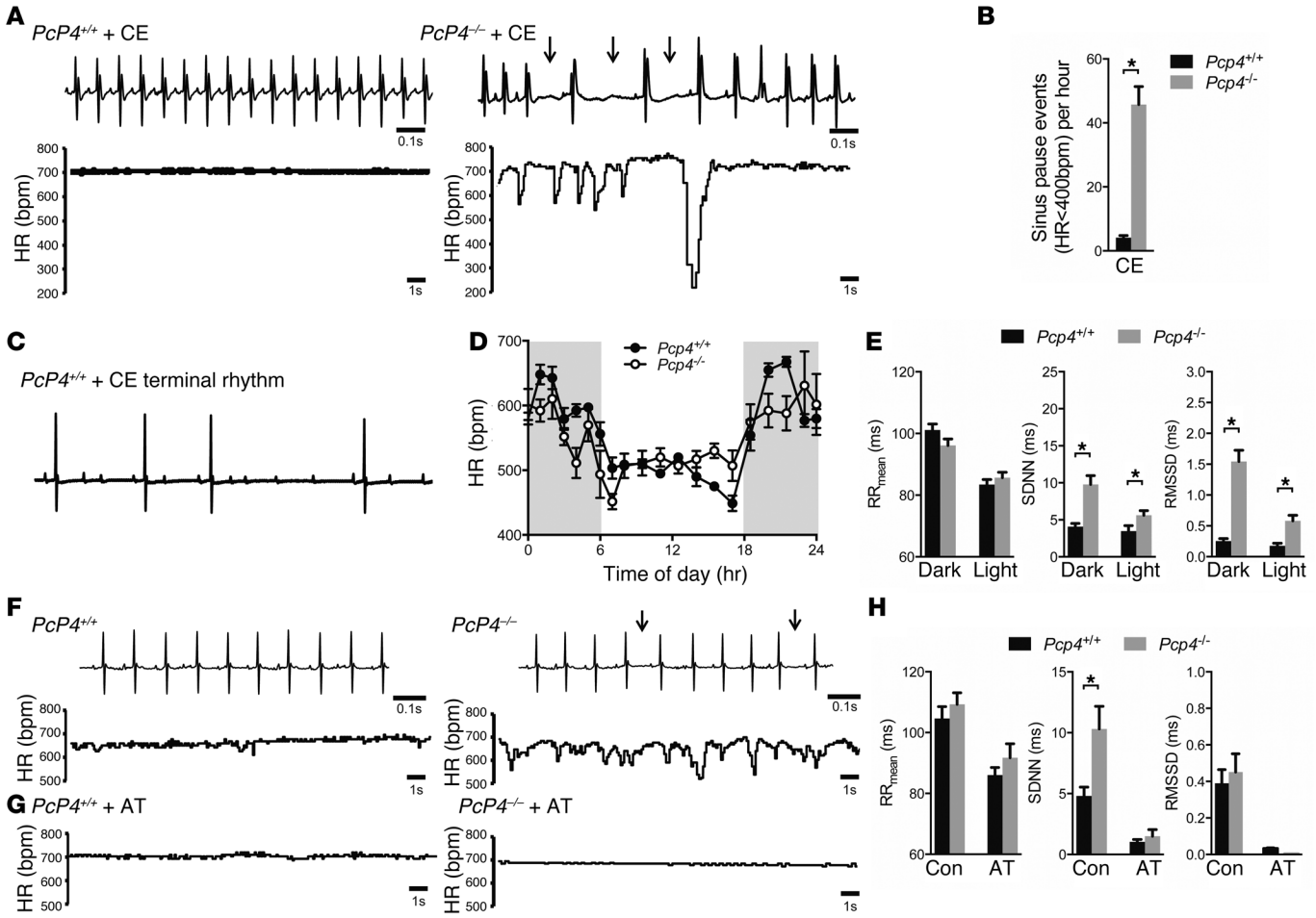

Figure 9. *Pcp4*-null mice are prone to vagally mediated arrhythmias. (**A**) Representative ECG tracings and graphical plot of heart rate in conscious telemetered mutant and WT mice after administration of caffeine and epinephrine. (**B**) Comparison of sinus pause events between mutant and WT mice after caffeine and epinephrine. (**C**) ECG tracing of terminal bradycardic rhythm during anesthesia withdrawal in *Pcp4*-null mouse treated with caffeine and epinephrine. (**D**) Telemetric recordings of average heart rate in *Pcp4*-null and control mice over a 24-hour period. (**E**) Comparison of average heart rate and time domain measures of HRV (SD of N-N intervals [SDNN]; root mean square of successive differences [RMSSD]) between conscious *Pcp4*-null and control mice. (**F** and **G**) Representative ECG tracings and graphical plot of heart rate in mutant and WT mice (**F**) at baseline, and (**G**) after administration of atropine (AT). Arrows denote prolonged R-R intervals. (**H**) Comparison of average heart rate and time domain measures of HRV between conscious *Pcp4*-null and control mice before (Con) and after administration of AT. Data represent mean ± SEM. $^*P < 0.05$.

The activation pulse protocol was as follows: holding potential –50 mV, a brief pulse to –30 mV for 30 ms to inactivate any Na current, then pulse to testing potential from –40 mV to +40 mV for 300 ms, with a 10-mV increment. The inactivation pulse protocol was as follows: with a series of holding potential from –60 mV to 15 mV for 1 s, with a 5-mV increment, then briefly prepulsed to –30 mV for 30 ms, then stepped to 0 mV.

Animal models. Cardiac disease was induced in mice with (a) transverse aortic constriction as previously described (33) for 6 weeks; or (b) PE (100 mg/kg body weight/d) delivered via s.c. osmotic minipump (Alzet) as previously described (34) for 1 week. For all immunohistochemistry experiments, WT C57BL/6 mice were used. For all functional studies, WT littermates of *Pcp4*-null animals bred into the *Cntn2-EGFP* background were used.

ECG monitoring, echocardiography, and drug testing. ECGs on anesthetized mice were performed as previously described (35). Echocardiograms were performed as previously described (36) (Vevo; FujiFilm VisualSonics Inc.). Telemetric ECGs were performed as previously described (37). HRV was assessed from 24-hour telemetric recordings in conscious mice as previously described (38). HRV and arrhythmia assessment were performed both before and within the 30-minute interval after administration of atropine (1 mg per kg body weight i.p.) or caffeine (120 mg per kg body weight i.p.) and epinephrine (2 mg per kg body weight i.p.). A subset of anesthetized mice ($n = 3$) that were given caffeine and epinephrine were administered atropine 5 minutes prior to recovery from anesthesia.

Statistics. AP characteristics, calcium currents, calcium transient parameters, the proportion of cells from a given heart displaying SCaEs, and immunofluorescent intensity were compared using Sidak 1-way ANOVA. $P < 0.05$ was considered significant.

Study approval. All experiments were performed according to protocols approved by the NYU School of Medicine Institutional Animal Care and Use Committee and conformed to the NIH guidelines for the care and use of laboratory animals. Protocols for studies

of cadaveric fetal human tissues were approved by the NYU Institutional Review Board.

Acknowledgments

This work was supported by grants from the NIH to G.I. Fishman (R01HL105983) and A. Shekhar (T32 GM066704). We are grateful to James I. Morgan for providing the *Pcp4*-null mouse line and the PCP4 antiserum.

Address correspondence to: Glenn I. Fishman, Leon H. Charney Division of Cardiology, NYU School of Medicine, 522 First Avenue, Smilow 801, New York, New York 10016, USA. Phone: 212.263.3967; E-mail: glenn.fishman@nyumc.org.

1. Haissaguerre M, et al. Mapping and ablation of ventricular fibrillation associated with long-QT and Brugada syndromes. *Circulation*. 2003;108(8):925–928.
2. Kang G, et al. Purkinje cells from RyR2 mutant mice are highly arrhythmogenic but responsive to targeted therapy. *Circ Res*. 2010;107(4):512–519.
3. Bansch D, et al. Successful catheter ablation of electrical storm after myocardial infarction. *Circulation*. 2003;108(24):3011–3016.
4. Sinha AM, et al. Role of left ventricular scar and Purkinje-like potentials during mapping and ablation of ventricular fibrillation in dilated cardiomyopathy. *Pacing Clin Electrophysiol*. 2009;32(3):286–290.
5. Boyden PA, Hirose M, Dun W. Cardiac Purkinje cells. *Heart Rhythm*. 2010;7(1):127–135.
6. Ideker RE, Kong W, Pogwizd S. Purkinje fibers and arrhythmias. *Pacing Clin Electrophysiol*. 2009;32(3):283–285.
7. Di Maio A, Ter Keurs HE, Franzini-Armstrong C. T-tubule profiles in Purkinje fibres of mammalian myocardium. *J Muscle Res Cell Motil*. 2007;28(2–3):115–121.
8. Shorofsky SR, January CT. L- and T-type Ca^{2+} channels in canine cardiac Purkinje cells. Single-channel demonstration of L-type Ca2+ window current. *Circ Res*. 1992;70(3):456–464.
9. Hirose M, Stuyvers B, Dun W, Ter Keurs H, Boyden PA. Wide long lasting perinuclear Ca^{2+} release events generated by an interaction between ryanodine and IP3 receptors in canine Purkinje cells. *J Mol Cell Cardiol*. 2008;45(2):176–184.
10. Vassalle M, Lin CI. Calcium overload and cardiac function. *J Biomed Sci*. 2004;11(5):542–565.
11. Cordeiro JM, Spitzer KW, Giles WR. Repolarizing K^+ currents in rabbit heart Purkinje cells. *J Physiol*. 1998;508(pt 3):811–823.
12. Vaidyanathan R, et al. The ionic bases of the action potential in isolated mouse cardiac Purkinje cell. *Heart Rhythm*. 2013;10(1):80–87.
13. Pallante BA, et al. Contactin-2 expression in the cardiac Purkinje fiber network. *Circ Arrhythm Electrophysiol*. 2010;3(2):186–194.
14. Li P, Rudy Y. A model of canine purkinje cell electrophysiology and Ca(2+) cycling: rate dependence, triggered activity, and comparison to ventricular myocytes. *Circ Res*. 2011;109(1):71–79.
15. Slemmon JR, Morgan JI, Fullerton SM, Danho W, Hilbush BS, Wengenack TM. Camstatins are peptide antagonists of calmodulin based upon a conserved structural motif in PEP-19, neurogranin, and neuromodulin. *J Biol Chem*. 1996;271(27):15911–15917.
16. Kleerekoper QK, Putkey JA. PEP-19, an intrinsically disordered regulator of calmodulin signaling. *J Biol Chem*. 2009;284(12):7455–7464.
17. Johanson RA, Sarau HM, Foley JJ, Slemmon JR. Calmodulin-binding peptide PEP-19 modulates activation of calmodulin kinase II In situ. *J Neurosci*. 2000;20(8):2860–2866.
18. Saimi Y, Kung C. Calmodulin as an ion channel subunit. *Annu Rev Physiol*. 2002;64:289–311.
19. Swaminathan PD, Purohit A, Hund TJ, Anderson ME. Calmodulin-dependent protein kinase II: linking heart failure and arrhythmias. *Circ Res*. 2012;110(12):1661–1677.
20. Crotti L, et al. Calmodulin mutations associated with recurrent cardiac arrest in infants. *Circulation*. 2013;127(9):1009–1017.
21. Nyegaard M, et al. Mutations in calmodulin cause ventricular tachycardia and sudden cardiac death. *Am J Hum Genet*. 2012;91(4):703–712.
22. Janiak R, Lewartowski B. Early after-depolarisations induced by noradrenaline may be initiated by calcium released from sarcoplasmic reticulum. *Mol Cell Biochem*. 1996;163–164:125–130.
23. Shiferaw Y, Aistrup GL, Wasserstrom JA. Intracellular Ca^{2+} waves, afterdepolarizations, and triggered arrhythmias. *Cardiovasc Res*. 2012;95(3):265–268.
24. Wehrens XH. CaMKII regulation of the cardiac ryanodine receptor and sarcoplasmic reticulum calcium release. *Heart Rhythm*. 2011;8(2):323–325.
25. Alkadhi KA, Alzoubi KH, Aleisa AM. Plasticity of synaptic transmission in autonomic ganglia. *Prog Neurobiol*. 2005;75(2):83–108.
26. Skold K, et al. Decreased striatal levels of PEP-19 following MPTP lesion in the mouse. *J Proteome Res*. 2006;5(2):262–269.
27. Utal AK, Stopka AL, Roy M, Coleman PD. PEP-19 immunohistochemistry defines the basal ganglia and associated structures in the adult human brain, and is dramatically reduced in Huntington's disease. *Neuroscience*. 1998;86(4):1055–1063.
28. Iwamoto K, Bundo M, Yamamoto M, Ozawa H, Saito T, Kato T. Decreased expression of NEFH and PCP4/PEP19 in the prefrontal cortex of alcoholics. *Neurosci Res*. 2004;49(4):379–385.
29. Kiriazis H, et al. Neurocardiac dysregulation and neurogenic arrhythmias in a transgenic mouse model of Huntington's disease. *J Physiol*. 2012;590(pt 22):5845–5860.
30. Gutstein DE, et al. Conduction slowing and sudden arrhythmic death in mice with cardiac-restricted inactivation of connexin43. *Circ Res*. 2001;88(3):333–339.
31. Madisen L, et al. A robust and high-throughput Cre reporting and characterization system for the whole mouse brain. *Nat Neurosci*. 2010;13(1):133–140.
32. Wei P, Blundon JA, Rong Y, Zakharenko SS, Morgan JI. Impaired locomotor learning and altered cerebellar synaptic plasticity in pep-19/PCP4-null mice. *Mol Cell Biol*. 2011;31(14):2838–2844.
33. Qu J, et al. Gap junction remodeling and spironolactone-dependent reverse remodeling in the hypertrophied heart. *Circ Res*. 2009;104(3):365–371.
34. Mori J, et al. Agonist-induced hypertrophy and diastolic dysfunction are associated with selective reduction in glucose oxidation: a metabolic contribution to heart failure with normal ejection fraction. *Circ Heart Fail*. 2012;5(4):493–503.
35. Sotoodehnia N, et al. Common variants in 22 loci are associated with QRS duration and cardiac ventricular conduction. *Nat Genet*. 2010;42(12):1068–1076.
36. Ram R, Mickelsen DM, Theodoropoulos C, Blaxall BC. New approaches in small animal echocardiography: imaging the sounds of silence. *Am J Physiol Heart Circ Physiol*. 2011;301(5):H1765–H1780.
37. Cerrone M, et al. Bidirectional ventricular tachycardia and fibrillation elicited in a knock-in mouse model carrier of a mutation in the cardiac ryanodine receptor. *Circ Res*. 2005;96(10):e77–e82.
38. Thireau J, Zhang BL, Poisson D, Babuty D. Heart rate variability in mice: a theoretical and practical guide. *Exp Physiol*. 2008;93(1):83–94.